Electronic states of neutral and ionized tetrahydrofuran studied by VUV spectroscopy and ab initio calculations

A. Giuliani, Paulo Limão-Vieira, D. Duflot, A. R. Milosavljevic, B. P. Marinkovic, S. V. Hoffmann, N. J. Mason, J. Delwiche, M.-J. Hubin-Franskin

Electronic states of neutral and ionized tetrahydrofuran studied by VUV spectroscopy and *ab initio* calculations

A. Giuliani [1,2,*], P. Limão-Vieira [3, 4], D. Duflot [5], A. R. Milosavljevic [6], B. P. Marinkovic [6], S. V. Hoffmann [7], N. Mason [4], J. Delwiche [8], M.-J. Hubin Franskin [8]

[1] DISCO beamline, Synchrotron Soleil, L'Orme des Merisiers, Saint-Aubin, 91192 Gif-sur-Yvette, France

[2] Cepia, Institut National de la Recherche Agronomique (INRA), BP 71627, 44316 Nantes Cedex 3, France

[3] Laboratório de Colisões Atómicas e Moleculares, CEFITEC, Departamento de Física, Universidade Nova de Lisboa, 2829-516 Caparica, Portugal

[4] Centre of Molecular and Optical Sciences, Department of Physics and Astronomy, The Open University, Walton Hall, Milton Keynes, MK7 6AA, UK

[5] Laboratoire de Physique des Lasers, Atomes et Molécules (PhLAM), UMR CNRS 8523, Centre d'Études et de Recherches Lasers et Applications (CERLA, FR CNRS 2416), Université des Sciences et Technologies de Lille, F-59655 Villeneuve d'Ascq Cedex, France

[6] Laboratory for atomic collision processes, Institute of Physics, Pregrevica118, 11080 Belgrade, Serbia

[7] Institute for Storage Ring Facilities, University of Aarhus, Ny Munkegade, DK-8000, Aarhus C, Denmark

[8] Laboratoire de Spectroscopie d'Électrons diffusés, Université de Liège, Institut de Chimie-Bât. B6c, B-4000 Liège 1, Belgium

[*] e-mail: alexandre.giuliani@synchrotron-soleil.fr

Abstract

The electronic spectroscopy of isolated tetrahydrofuran (THF) in the gas phase has been investigated using high-resolution photoabsorption spectroscopy in the 5.8-10.6 eV with absolute cross section measurements derived. In addition, an electron energy loss spectrum was recorded at 100 eV and 10° over the 5-11.4 eV range. The He(I) photoelectron spectrum was also collected to quantify ionisation energies in the 9-16.1 eV spectral region. These experiments are supported by the first high-level *ab initio* calculations performed on the excited states of the neutral molecule and on the ground state of the positive ion. The excellent agreement between the theoretical results and the measurements allows us to solve several discrepancies concerning the electronic state spectroscopy of THF. The present work reconsiders the question of the lowest energy conformers of the molecule and its population distribution at room temperature.

PACS. 33.20.Ni – 33.60.+q – 32.80.Ee – 31.15.A- – 87.53.j

1. Introduction

Tetrahydrofuran (THF) is a five membered heterocyclic ring that is often used as a chemical and molecular model for the (deoxy)ribose ring in nucleic acids. In the past ten years considerable research has been dedicated to the study of the spectroscopy and collisional interactions with biomolecules such as THF - either deposited as thin films or in the gas phase. The motivation for much of this work has been in relation to the study of radiation damage to biomolecules since it is known that a large amount of the energy deposited in biological media by ionising radiation is channelled into biomolecules such as DNA and the lipids forming cellular membranes. In particular ionising radiation liberates large numbers of low energy secondary electrons [1]. These secondary electrons, despite having energies below the ionization threshold, can induce significant amounts of both single and double strand breaks within the cellular DNA [2] in turn providing the origin of mutations or inducing cellular death [3].

Low energy electrons may also excite biomolecular targets through inelastic collisions and populate electronically excited states which may subsequently decay with the production of 'radicals' whose chemical reactivity may strongly influence the local site chemistry. A detailed understanding of the electronic state spectroscopy of the molecular constituents of DNA are therefore necessary if we are to develop a comprehensive understanding of radiation induced damage in DNA at a molecular level. However since the nucleosides and nucleotides comprising DNA are solids at room temperature it has, to date, proven difficult to measure absolute photoabsorption cross sections for these compounds and to date there are only a few spectroscopic studies of such molecules. THF provides a good analogue for the (deoxy)ribose nucleic acids and therefore in recent years has been the subject of several experimental and theoretical studies [4-15]. However severe discrepancies concerning the spectroscopy of THF remain.

THF is a puckered molecule supporting several internal motions of out-of-plane ring vibrations, called pseudorotation [16]. The molecule may adopt several different conformations, Fig. 1, all of which appear to be connected along the pseudorotation path as a function of the pseudorotation angle ϕ. A similar type of ring deformation is known to occur in the nucleosides and nucleotides and is closely related to higher order structure in the nucleic acids like DNA and RNA [17]. The preferred conformation of the isolated molecule in the gas phase is still debated, despite several experimental [18-21] and theoretical studies to

clarify the situation [16,21-24]. Recently, Yang *at al.* suggested that the most populated conformer could be obtained from Electron Momentum Spectroscopy (EMS) [25].

The first study of the electronic state spectroscopy of THF was performed by Picket *et al.* [26], who measured the VUV photoabsorption spectrum for the first time. This early work reported two electronic transitions at 51440 cm^{-1} (6.378 eV) and 55640 cm^{-1} (6.899 eV). Subsequent work by Hernandez [27] confirmed the electronic transitions of Pickett *et al.* [26]. A vibrational analysis of structure observed in the VUV spectrum was performed and four Rydberg series identified. Subsequently Davidson *et al.* [28] contested these pioneering investigations. They suggested the lowest energy optically active transition to be the $n \rightarrow 3s$ transition [28] at 6.03 eV. A complex vibrational structure was reported involving multiple excitations and de-excitation of the pseudo-rotation mode with frequencies ranging from 60 to 260 cm^{-1} [28]. Above 6.3 eV the band broadens and a second electronic transition was suggested with vibrational frequencies around 200 cm^{-1}. The presence of such an unexpected transition in this energy region was commented upon by Robin [29]. Tam and Brion have recorded the first electron energy loss spectrum in dipolar excitation conditions of the molecule [30]. Their analysis of the spectral band was based on derived term values. A Rydberg series analysis by Doucet *et al* [31] reported a single ns series ($\delta = 0.94$), two np series ($\delta = 0.64$ and 0.52) and a single nd series ($\delta = 0.08$). Their assignment of the n = 3 member was in agreement with the previous work, but interestingly, their vibrational analysis of the first spectral band did not involve a second electronic origin. Bremner *et al*. [32] re-examined the VUV photoabsorption spectrum of THF extending the excitation energy range up to the LiF cut off at 11.8 eV allowing further Rydberg series to be analysed.

In this paper we present a combined theoretical and experimental study of the ground and excited states of both the neutral THF molecule and its cation. We believe that this work represents the highest resolution photoabsorption and photoelectron data currently available. For the first time, the neutral and ionic excited states are studied theoretically using high-level *ab initio* methods. Through a combination of these theoretical and experimental results we are then able to discuss previous discrepancies concerning the nature of the lowest energy spectral band in the photoabsorption and reassign the broad features at higher energies. This, in turn, leads us to address the question of the lowest energy conformers of the molecule and to question the claims of Yang *et al.* [25] following their EMS study. Hitherto, the electronic

spectra of THF recorded at room temperature were interpreted on the basis of a single geometry. We show in the following that a better description of the electronic spectroscopy of the molecule is gained by considering the two lowest energy conformers.

2. Methods

2.1. Photoabsorption spectroscopy

The high-resolution VUV photoabsorption measurements were performed using the ASTRID – UV1 beam line at the Institute for Storage Ring Facilities (ISA), University of Aarhus, Denmark. A detailed description of the apparatus can be found elsewhere [33], so only a brief description will be given here. A toroidal dispersion grating is used to select the synchrotron radiation with a FWHM wavelength resolution of approximately 0.075 nm. The synchrotron radiation passes through the static gas sample at room temperature. A photo-multiplier is used to detect the transmitted light. For wavelengths below 200 nm a flow of He gas is flushed through the small gap between the photomultiplier and the exit window of the gas cell to prevent any absorption by air in the VUV range of the spectrum. A LiF entrance window acts as an edge filter for higher order radiation restricting the photoabsorption measures to below 10.8 eV (115 nm). The grating itself provides a maximum wavelength (lower energy limit) of 320 nm (3.9 eV). The sample pressure is measured by a Baratron capacitance gauge. To avoid any saturation effects sample pressures were chosen such that the transmitted flux was > 10% of the incident flux.

Gas transmission results are compared to a background scan recorded with an evacuated cell. Absolute photoabsorption cross sections may then be calculated using the Beer-Lambert law:

$$I_t = I_0 \exp(-n\sigma x),$$

where I_t is the intensity of the light transmitted through the gas sample, I_0 is that through the evacuated cell, n is the molecular number density of the sample gas, σ is the absolute photoabsorption cross section and x is the absorption path length (25 cm). The accuracy of the absolute cross-section is estimated to be better than 5%.

2.2. Photoelectron spectroscopy

He(I) (21.22eV) photoelectron spectra of THF were recorded at the Université de Liège, Belgium. The apparatus has been described in detail previously [34]. Briefly, the spectrometer consists of a 180° cylindrical electrostatic analyser with a mean radius of 5 cm. The analyser

is used in constant energy pass mode. The incident photons are produced by a D.C. discharge in a two-stage differentially pumped lamp. The energy scale was calibrated using argon lines ($^2P_{3/2}$ = 15.760 eV and $^2P_{1/2}$ = 15.937 eV) [35,36] and the resolution of the present spectrum is measured from the full width half maximum of the Ar peaks to be 50 meV, in presence of THF. The intensities in the spectrum were corrected for the transmission of the analyzing system. The data reported here are the sums of many individual spectra. This procedure allows us to obtain a good signal-to-noise ratio while keeping the pressure in the spectrometer at very low level (< 5×10^{-6} mbar). The accuracy of the energy scale is estimated to be ± 2 meV.

2.3. Electron energy loss spectroscopy

The electron energy loss spectra of THF have been measured at the Institute of Physics, Belgrade, using a cross beam experimental setup which has been described recently [37]. Briefly, a non-monochromated electron beam produced by an electron gun crosses perpendicularly a molecular beam produced by a non-magnetic stainless steel needle. The scattered electrons are retarded and focused into a double cylindrical mirror energy analyzer (DCMA). After being selected by energy, the electrons are focused by a three-element cylindrical lens into a single channel multiplier, working in a single counting mode. The highest energy resolution was limited by the initial thermal spread of incident electrons to be about 0.5 eV. The accuracy of the incident electron energy was determined to be ±0.4 eV by observing a threshold for He^+ ions yield. The electron gun can be rotated around the gas needle in the range of about -40^o to 130^o. The uncertainty of the angular scale was found to be better than ±0.5^o. The base pressure was about $3x10^{-7}$ mbar and the operating pressure was about $6x10^{-6}$ mbar. The electron energy loss measurements were performed in a constant pass energy mode, by ramping the retarding potential at the entrance of DCMA. The calibration of the energy loss scale has been obtained according to the position of the elastic peak. The measurements were performed in conditions that favor dipole-allowed transitions – small scattering angles (10°) and high incident energies (100 eV), such that they may be directly compared with the high-resolution VUV optical measurements.

2.4. The terahydrofuran sample

The gas sample used in all the measurements was purchased from Sigma-Aldrich, with a minimum purity of +99%. The samples have been submitted to repeated freeze-pump-thaw cycles to remove the dissolved gases.

2.5. *Ab initio* calculations

Ab initio calculations were used to determine vertical excitation energies of the electronic states using the EOM-CCSD [38] implemented in the MOLPRO programme [39]. The equilibrium geometry of the C_2 and C_s conformers is identical to the results of Rayón and Sordo [24] obtained at the MP2 level with the aug-cc-pVDZ basis set. In order to describe Rydberg states, diffuse functions (5s, 5p, 5d) taken from Kaufmann *et al*. [40] were added at the centre of the molecule . The ionisation energies were obtained with the Restricted Outer Valence Green's Function (ROVGF) method [41, 42], using the Gaussian03 package [43].

3. Results and Discussion

3.1. Neutral ground state

As mentioned in the introduction, the lowest energy structure of the molecule is still the subject of debate. Table 1 summarizes the literature results together with the present findings. According to the microwave spectroscopic studies of Mamleev *et al*. [20], supported by the recent experimental and theoretical work of Melnik *et al.* [21], the global minimum is found for the twisted C_2 conformation. These findings are in sharp contrast with the previous results of Engerholm *et al.* [18] and of Meyer *et al.* [19], for whom the global minimum is very close to the envelope ${}_5E$ (C_1) conformation. From a theoretical point of view Cadioli *et al.* [22] using HF and MP2 calculation found C_2, C_1 and C_s in this increasing sequence stability. Han and Kang [23] reported at the HF and MP2 level of theory the twisted C_2 conformations to be the most stable. Melnik *et al.* [21] carried out MP2/6-31+G(p,d) and B3LYP/6-31+G(p,d) calculations, which gave the twisted C_2 as a global minimum in perfect agreement with their experimental results. Wu and Cremer also reported, at the MP2/cc-pVTZ and B3LYP/6-31G(p, d) levels, the twisted ${}_1E$ geometry (C_2) to be the global minimum [16] lying ~0.2 kcal/mol below the C_s geometry. Recently, Rayón and Sordo [24] performed a detailed theoretical study at the MP2/aug-cc-pVTZ including anharmonic ZPE correction and suggested that the envelopes C_s are the global minima structures. The authors estimated the energy difference between C_s and C_2 minima to be 46 cm^{-1} (i.e. 0.13 kcal/mol) at the CCSD(T)//CBS(MP2) level. Surprisingly, this theoretical finding is at variance with every previous result from microwave spectroscopy and from theoretical calculations as seen in Table 1. It is also worth noting that, as previously mentioned by Cadioli *et al.* [22], results from X-rays [44] and neutron diffraction [45] experiments are consistent with the C_2 geometry, as seen from the values of dihedral angle involving the ring at supplementary

information table 1. Rayón and Sordo [24] have pointed out that the potential energy surface (PES) is nearly flat, which makes the characterisation of geometries as the extrema along the pseudo-rotational coordinate a challenging task. The global shape of the PES was also found to be extremely dependent on the basis set used. Recently, from EMS experiments, Yang *et al.* [25] have claimed the C_s geometry to be the most populated conformer of THF on the basis on better agreement of calculated orbital momentum distribution for the C_s geometry with the experiment.

We have calculated the ground state geometry at the MP2 level of theory following Rayón and Sordo [24] for the C_{2v}, C_2 and C_s isomers (the C_1 isomer being neglected) using the aug-cc-pVDZ basis set. The results are compared with the available literature data [19,22-24,44,45] at supplementary information, table 1. At this level, the C_s geometry is a saddle point but with the larger aug-cc-pVTZ basis set C_s and C_2 are minima of the PES. Although the basis set has been found by Rayón and Sordo [24] to have important effects on the nature of the PES extremum, our use of the aug-cc-pVDZ basis set should have little influence on the electronic excitation energies, especially since most excited states are Rydberg in nature. Considering the Rayón and Sordo computed energy separation of 46 cm^{-1} for these two lowest energy conformers, it is very likely that at room temperature both isomers coexist. Indeed, a Boltzmann analysis at 298 K indicates that C_2 and C_s amount to 55.5 % and 44.5 % of the population, respectively. The C_{2v} geometry is excluded from the Boltzmann population analysis since a consensus has been reached in the literature, for which this geometry is a saddle point [19,22-24,44,45] with two imaginary frequencies. We shall therefore consider in the following discussion the possible spectral signature from the C_s and C_2 conformers of THF.

The electronic configuration of THF in its electronic ground state and in the C_{2v} formalism is: $1a_1^2 1b_2^2 2a_1^2 3a_1^2 2b_2^2 4a_1^2 5a_1^2 3b_2^2 6a_1^2 4b_2^2 1b_1^2 7a_1^2 1a_2^2 2b_1^2 5b_2^2 8a_1^2 6b_2^2 9a_1^2 2a_2^2 3b_1^2 : \quad \tilde{X}\,^1A_1$.

C_{2v} correlates unambiguously to the other lower geometries. In the C_2 point group, the C_{2v} a_1 and a_2 become a and b_1 and b_2 correlate to b. For the C_s geometry, a_1 and b_1 become a′and a_2 and b_2 become a″.

The molecule possesses 33 normal vibrations distributed into two irreducible subgroups 17A+16B in the C_2 point group [22,23, 46, 47]. The literature data on the normal vibrational mode are shown in supplementary information table 2 together with the assignments from Lepage *et al.* [4].

3.2. Neutral excited states

Table 2 compares the calculated excited states transition for the two lowest energy geometries of THF, namely C_s and C_2, with the assignments made from the photoabsorption measurements. Figure 2 shows the photoabsorption spectrum recorded between 5.8 eV and 10.7 eV (2a) and the electron energy loss spectra (EELS) up to 11.5 eV (2b). Although measured at lower resolution, the EELS spectra agree well with the photoabsorption data for the band position. Our data also appears to be in very good agreement with the literature data of Davidson *et al.* [28] and Bremner *et al.* [32] in both energy position and absolute cross section, although our resolution is better than that of Bremner *et al.* [32]. The photoabsorption spectrum is composed of a low energy band peaking at 6.6 eV, on which very sharp features are superimposed. At 6.9 eV a second band starts and extending up to 7.7 eV, peaking at 7.15 eV with a local maximum cross section of 12 Mbarn. This band also shows structure on its low energy side. It is followed by a third band up to 8.3 eV on which sharper features are observed. From 8.3 eV, the cross section, superimposed with sharper features, rises almost monotonically up to the end of the present measurements.

3.2.1. Lowest energy excited states

3.2.1.1. The 3s terms of the series converging to the ionic ground electronic state

Figure 3(a) shows the lowest energy band spanning from 6.04 to 6.88 eV. This spectral region appears extremely structured. As discussed above, the assignments to be given to this band have been much debated in the literature and there is currently no agreement as to its classification. Davidson *et al.* [28], on the basis of careful vibrational analysis conducted at different sample temperatures, concluded that this band should be assigned to two electronic origins with their associated vibrational progressions. In contrast other authors reported a single electronic transition with heavy hot band structure. This absorption band, centred around 6.5 eV, which corresponds to a term value of 3.25 eV is indicative of a 3s-type Rydberg state. Hence, the presence of two electronic origins was puzzling, as noted by Robin [29].

Our calculations (table 2) predict the lowest energy singlet excited state of the molecule to be the 3s Rydberg state converging to the first ionic limit for every geometry considered. Vertical transition to this excited state is calculated at a noticeable lower energy (6.357 eV) but with half the oscillator strength for the C_2 geometry than for the C_s (6.608 eV). Hence, based on our theoretical results, we assign the first absorption band to the lowest energy

transitions for the C_2 and C_s conformers, see Fig. 3(a). We have placed the 3s(C_2) adiabatic transition energy at 6.221 eV in agreement with Davidson *et al.* [28]. The vibrational assignments are given in supplementary information table 3. The vibrational structure may be rationalized in terms of a progression of 62.9 cm^{-1} **(**7.8 meV) corresponding to the excitation of the ring-puckering mode (table 1). We estimate the vertical energy for the 3s(C_2) transition to be around 6.3 eV. In agreement with Davidson *et al*. [28] we find a hot band system involving excitation of ν_{17}, which wavenumber of 250.8 cm^{-1} (31.1 meV) agrees very well with the values reported for the ground state of 286 cm^{-1} (35.5 meV) (see table 3 and also in supplementary information).

The 3s(C_s) 0-0 transition is placed at 6.353 eV and appears accompanied by two long and overlapping progressions of 171 cm^{-1} (21.2 meV) and 237 cm^{-1} (29.38 meV) assigned to the ring-puckering modes ν_{33} and ν_{17}, respectively (see table 3 and also in supplementary information). The ν_{33} progression was also reported by Davidson *et al.* [28] but with no further discussion.

3.2.1.2.The 3p terms of the series converging to the ionic ground electronic state

Figure 3(b) shows an enlargement of the 6.8 to 8.4 eV band system. Our calculations predict excitations of the 3p members to be mostly responsible for this absorption band, in agreement with the previous work of Bremner *et al.* [32]. Again, the agreement between theory and experiment is excellent and allows a straightforward interpretation of this spectral region. The calculation predicts the 3p excitation for the C_s geometry at 7.154 eV with oscillator strength of 0.047, which is very close to the maximum of the absorption band at 7.19 eV. This feature was assigned to excitation of a 3p state by Bremner *et al.* [32]. The maximum of this band appears structured by less intense and sharp features, which are assigned to vibrational excitation accompanying this electronic transition. Analysis of this fine structure leads us to place the electronic origin at 7.134 eV. We identify a single progression of vibrational modes of 79.8 cm^{-1} (9.9 meV) assigned to ring-puckering vibrations ν_{33}, (Table 3 and supplementary information Table 4). The two remaining 3p transitions for the C_s conformer are expected at slightly higher energy but with lower intensity. The 7.3 eV feature does not fit into the vibrational progression of the first 3p(C_s) transition. Hence, it is likely that this peak corresponds to the adiabatic transition of the 3p(C_s) transition predicted at 7.296 eV. A single member of a progression involving excitation of a 136.3 cm^{-1} (16.9 meV) mode is also observed (Table 3 and supplementary information Table 4). On the higher energy side

of the absorption band, a poorly resolved feature appears at 7.35 eV. It could arise from the excitation of the third 3p(C_s) member calculated at 7.381 eV. This electronic transition is also accompanied by excitation of the ν_{33} mode with 185.5 cm^{-1} (23 meV) (Table 3 and supplementary information Table 4).

On the low energy side of this absorption band, another structure is observed, which does not fit into the progression associated with the first 3p(C_s) transition. As seen in Table 2, the calculation predicts a 3p transition for the C_2 conformer at lower energy than the 3p(C_s), but with appreciably lower oscillator strength. The two other 3p(C_2) transitions are predicted to have negligible oscillator strength. The maximum of this transition may be estimated from the photoabsorption spectrum (Fig. 3b) at 7.03 eV, which fits very well with the theoretical prediction at 7.103 eV for the 3p(C_2). We assign the electronic origin of the 3p(C_2) transition to the 6.898 eV feature. The progressions identified involve excitation of 183.9 cm^{-1} (22.8 meV) vibrational mode, which we assign to the ring-puckering ν_{33} modes of this excited states. Associated with the electronic origin is a hot band involving excitation of a 277.5 cm^{-1} (34.4 meV) mode, which is consistent with the ν_{17} wavenumber in the ground state (Table 3 and supplementary information Table 4). Our vibrational assignments for this band are in disagreement with those of Bremner *et al.* [32]. These authors have looked for a vibrational spacing similar to that observed in the photoelectron spectrum. Indeed, Rydberg states are known to exhibit similar features to the ion to which they converge. We have not followed this procedure in the present case. The computed $\langle r^2 \rangle$ (Table 2) for the 3p states involved are similar in magnitude to those computed for the 3s states for which the vibrational progression are very different from those reported for the ionic ground state (see below). Moreover, the higher resolution of the present data allows us to resolve for the first time fine features on top of the 7.2 eV band (Fig. 2, 3), which were not observed by Bremner *et al.* [34].

3.2.1.3. The 3d terms of the series converging to the ionic ground electronic state

Similar to the 3s and 3p series, excitation of the first 3d members is predicted to occur at a noticeably lower energy for the C_2 conformer than for the C_2. Hence, Table 2 shows that the first 3d(C_2) state should be expected on the high-energy side of the 3p absorption band. As seen in Fig. 3b**,** a broad feature is observed at 7.483 eV, not well resolved from the underlying background but which agrees with the theoretical value of 7.474 eV for the excitation of the 3d(C_2) state. The spectral region extending from 7.40 eV to 8.15 eV is predicted to contain the 3d transitions for both conformers, which are computed to account for most of the

oscillator strength (Table 2). An enlargement of the spectrum shows a congested spectral region with quite sharp features. Two intense features are observed at 7.730 eV and 7.813 eV (Fig. 3b). These values match the predicted transition energies to two 3d(C_2) states at 7.715 eV and 7.754 eV. Following Bremner *et al.* [32], in searching for vibrational progression associated with these origins, it appeared that the shapes of these bands matched the first band of the photoelectron spectrum. The difference with the previous Rydberg states lies in greater $\langle r^2 \rangle$ values, as seen at Table 2. This more diffuse character explains the resemblance of these states with the ionic core. The vibrational assignments are summarized in Table 3 with also supplementary information Table 5.

A feature located at 7.749 eV and poorly resolved from the 7.730 eV peak is assigned to the lowest energy 3d(C_s) transition, on the basis of its computed value of 7.724 eV. The remaining 3d(C_s) excitations are predicted to be grouped around 8 eV but dominated by an intense excitation. We tentatively assign this excitation to the 7.867 eV feature, appearing as a shoulder on the 7.973 eV peak.

3.2.2. Higher excited states

The spectral region spanning from 8.2 to 10.6 eV is shown in Fig. 4. Table 4 shows our assignments of features attributable to Rydberg series converging to the first three ionisation limits. We report a single member of the ns series converging to the first ionisation limit for both conformers. The computed oscillator strengths for higher members of the progression are in every case too low to be observed (see Table 2). This result is in agreement with Bremner *et al.* [32]. Interestingly, the calculation predicts more intense np members ($n > 3$) for the C_s isomer. Our assignments follow from that and we report members up to $n = 5$ for the np series of the C_s isomers converging to the first ionic limit. The $n = 4$ members have δ values consistent with np excitations. We tentatively assign 5p members on the basis of the calculations, despite quantum defect values not being in perfect agreement with this assignment. Bremner *et al.* [32] report a single 5p member at 8.89 eV. We also report this member at 8.888 eV along with another one at 8.939.

For the C_2 isomer, nd series have been assigned up to $n = 9$, with consistent quantum defects. For the C_s isomer, nd series are reported up to $n = 7$. These assignments, although at variance

with the report of Bremner *et al.* [32] of two 3d series, are guided by the theoretical calculations.

Series converging to the second ionisation limit are reported for the C_2 isomer only. In agreement with Bremner *et al.* [32] and guided by the present calculations, we place a 3s series at ~ 8.3 eV. Moreover, we report two 3p series and a single 3d series, for the first time. The calculation predicts a 3s(C_2) and a 3p(C_s) converging to the third ionisation limit with noticeable oscillator strength. These members have been respectively assigned to the features at 8.965 eV and 9.037 eV with δ values of 0.870 and 0.655 supporting these assignments.

3.3. Ionic states

The He(I) photoelectron spectrum of THF is shown at Fig. 5(a). The ionic states have been calculated using the Outer Valence Green's Function (OVGF)/aug-ccp VDZ method. Table 5 shows the results for the C_s and C_2 conformers of the ground electronic state that were considered in this work, and compared with previous theoretical and experimental data. Our experimental results are in good agreement with those of Yang *et al*. [25], Kimura *et al.* [48] and Yamauchi *et al.* [49] where they overlap. Nevertheless, this work reports experimental ionisation energies with higher precision and the highest level of theoretical description. The ordering of the OVGF ionisation energies is in agreement with those of Yang *et al.* [25] except for the C_s conformer for which several discrepancies are found.

We have calculated the geometries of the ionic ground states at the UMP2/aug-cc-pVDZ level. It appears that, starting from the C_2 geometry of the ground electronic state, the $\tilde{X}^2$B state remains C_2 in nature with all its vibrational frequencies real (see supplementary information table 6). In contrast when the corresponding doublet is considered for the C_s conformer ($\tilde{X}^2$A′), the calculation converges towards the C_{2v} geometry. The computed vibrational frequencies for C_{2v} give one imaginary A_2 mode (ν_{17}) of 188 cm^{-1} (23.3 meV), which breaks the symmetry towards C_2. Hence, the topology of the ionic ground state potential energy surface is the following: two equivalent C_2 geometries separated by a C_{2v} saddle point giving a barrier of 1093.1 cm^{-1} (calculated with ZPE correction). The geometrical parameters for the C_2 and C_{2v} conformers of the positive ion are given at supplementary information table 1.

The first band of the photoelectron spectrum, shown at figure 5(b), extends from 9.3 to 10.3 eV. It appears to be composed (with the present 50 meV resolution) of a first feature peaking at 9.433 eV not completely resolved from a broader one on its high energy side. This band contains at least three features at 9.586 eV, 9.66 eV and 9.718 eV, which were not reported by Yang *et al*. [25]. The adiabatic transition is assigned to 9.433 eV. We assign the 9.586 eV feature to vibrational excitation involving one quantum of mode ν_{26} with 1234 cm^{-1}, which agrees well with the computed value of 1243.3 cm^{-1} (154 meV) for the C_s geometry. This mode also is found combined with ν_{32} and ν_{11} at 596.8 (74 meV) and 1064.7 cm^{-1} (132 meV) at 9.66 eV and 9.718 eV. These wavenumbers are consistent with excitations of reported values for the neutral ground state. Values are gathered in table 3 and supplementary information table 7.

According to the theoretical prediction, the ionisation energy of the C_s isomer is lower than that of the C_2 by 34 meV. We cannot resolve at the present experimental resolution two transitions so close in energy. Hence it is very likely that the two electronic origins for the C_2 and C_s isomers are superimposed and both contribute to the 9.433 eV peak.

The energy resolution of the electron momentum spectroscopy of Yang *et al*. [25] is around 1 eV [50]. This resolution is too poor to allow Yang *et al.* [25] to resolve the vibrational excitations associated with excitation of the ground ionic state we report. *A fortiori*, they cannot separate the contribution from the two major conformers of THF, which appear undistinguishable at the present 50 meV resolution.

4. Conclusions

This paper revisits the electronic spectroscopy of THF in the light of the first *ab initio* calculations ever performed to our knowledge on the excited states of the neutral molecule.
On the basis of the excellent agreement between the calculations and the measurements, we report that the experimental spectrum is composite and contains electronic excitations from both C_s and C_2 conformers of THF. Hence, this provides a solution to previous discrepancies in the literature concerning the nature of the lowest energy transitions for the molecule. The electronic spectrum has been re-examined up to 10.3 eV and new vibrational progression reported for the 3p and 3d Rydberg states. Higher members of Rydberg series are re-assigned in the light of the calculations.

The lowest energy part of the photoelectron spectrum is reported and an accurate value for the lowest adiabatic ionisation energy is reported. Calculations predict adiabatic transition to the ionic ground state to be separated by 34 meV for the two C_2 and C_s lowest energy conformers of the THF such that the present experimental resolution cannot resolve the separate contribution of the two conformers. Yang *et al.* [25] have reported experimental orbital momentum distribution for the HOMO of THF and compared these data to simulated distribution for the C_2 and C_s isomers. Since better agreement of the simulated distribution was obtained for the C_s isomer, the authors concluded the most stable conformer of THF to be the C_s one. Our work seems to indicate that both conformers coexist in the gas phase at room temperature and might be observed. Consequently, we question the conclusions of Yang *et al.* [25] about the reliability of their methodology to provide a new diagnostic for the most populated conformer of THF in the gas phase at room temperature.

5. Acknowledgments

We wish to thank the ISA at Aarhus,Denmark for access to the Astrid synchrotron under the EU FP6 programme IA-SFS contract number R113-CT-2004-506008. We also acknowledge support from the ESF EIPAM and ESF COST Action P9 (RADAM). We thank Pr Jose A. Sordo for providing details on his calculations. ARM and BPM acknowledge the support of the Ministry of Science of Republic of Serbia under Project No. 141011. The "PhLAM" is "Unité Mixte de Recherche du CNRS". The "Centre d'Études et de Recherches Lasers et Applications" (CERLA, FR CNRS 2416) is supported by the "Ministère chargé de la Recherche", the "Région Nord/Pas-de-Calais" and the "Fonds Européen de Développement Économique des Régions" (FEDER). The computations were carried out at the CRI (Centre de Ressources Informatiques), on the IBM computer which is supported by the "Programme de Calcul Intensif et Parallèle" of the "Ministère chargé de la Recherche", the "Région Nord/Pas-de-Calais" and the FEDER. NJM wishes to thank the UK EPSRC for financial support. PLV acknowledges the honorary research fellow position at University College London, the visiting fellow position at CEMOS, The Open University, UK, and together with M-J H-F the financial support from the Portuguese-Belgian joint collaboration. The Patrimoine of the University of Liège, the Fonds de la Recherche Scientifique (FRS-FNRS) and the Fonds de la Recherche Fondamentale Collective of Belgium have supported this research. M-J H-F wishes to acknowledge the Fonds de la Recherche Scientifique for

position. PLV and NJM acknowledge the support from the British Council for the Portuguese-English joint collaboration.

6. References

1. L. Sanche, Eur. J. Phys. D **35,** 367 (2005)
2. B. Boudaiffa, P. Cloutier, D. Hunting, M. A. Huels, L. Sanche, Science **287**, 1658 (2000)
3. C. von Sonntag, in *The Chemical Basis for Radiation Biology*, (Francis, London, 1987)
4. M. Lepage, S. Letarte, M. Michaud, F. Motte-Tollet, M.-J. Hubin-Franskin, D. Roy, L. Sanche, J. Chem. Phys. **109**, 5980 (1998)
5. D. Antic, L. Parenteau, M. Lepage, L. Sanche, J. Phys. Chem. B **103**, 6611 (1999)
6. D. Antic, L. Parenteau, L. Sanche, J. Phys. Chem. B **104**, 4711 (2000)
7. S.-P. Breton, M. Michaud, C. Jäggle, P. Swiderek, L. Sanche, J. Chem. Phys. **121**, 11240 (2004)
8. A. R. Milosavljevic, A. Giuliani, D. Sevic, M.-J. Hubin-Franskin, B. P. Marinkovic, Eur. J. Phys. D **35**, 411 (2005)
9. Zecca, C. Perazzolli, M. J. Brunger, J. Phys. B **38**, 2079 (2005)
10. P. Mozejko, L. Sanche, Radiat. Phys. Chem. **73**, 77 (2005)
11. D. Bouchiha, J. D. Gorfinkiel, L. G. Caron, L. Sanche, J. Phys. B **39**, 975 (2006)
12. C. S. Trevisan, A. E. Orel, T. N. Rescigno, J. Phys. B **39**, L255 (2006)
13. C. Winstead, V. McKoy, J. Chem. Phys. **125,** 074302 (2006)
14. Y. S. Park, H. Cho, L. Parenteau, A. D. Bass, L. Sanche, J. Chem. Phys. **125,** 074714 (2006)
15. P. Sulzer, S. Ptasinska, F. Zappa, B. Mielewska, A. R. Milosavljevic, P. Scheier, T. Mark, J. Chem. Phys. **125**, 044304 (2006)
16. A. Wu, D. Cremer, Int. J. Mol. Sci. **4**, 158 (2003)
17. W. Saenger, in *Principle of Nucleic Acid Structu*re, (Springer-Verlag, New York, 1984)
18. G. G. Engerholm, A. C. Luntz, W. D. Gwinn, D. O. Harris, J. Chem. Phys. **50**, 2446 (1969)
19. R. Meyer, J. C. Lopez, J. L. Alonso, S. Melandri, P. G. Favero, W. Caminati, J. Chem. Phys. **111**, 7871 (1999)
20. A. H. Mamleev, L. N. Gunderova, R. V. Galley, J. Struct. Chem. **42**, 365 (2001)
21. D. G. Melnik, S. Gopalakrishnan, T. A. Miller, J. Chem. Phys. **118**, 3589 (2003)
22. B. Cadioli, E. Gallinella, C. Coulombeau, H. Jobic, G. Berthier, J. Phys. Chem. **97**, 7844 (1993)
23. S. J. Han, Y. K. Kang, J. Mol. Struct. : THEOCHEM **369**, 157 (1996)
24. V. M. Rayón, J. A. Sordo, J. Chem. Phys. **122**, 204303 (2005)
25. T. Yang, G. Su, C. Ning, J. Deng, F. Wang, S. Zhang, X. Ren, Y. Huang, J. Chem. Phys. **111**, 4927 (2007)
26. L. W. Pickett, N. J. Hoeflich, T. C. Liu, J. Am. Chem. Soc. **73** (1951) 4865
27. G. J. Hernandez, J. Chem. Phys. **38**, 2233 (1963)
28. R. Davidson, J. Høg, P. A. Warsop, J. A. B. Whiteside, J. Chem. Soc. Faraday II **68**, 1652 (1972)
29. M. B. Robin, *Higher Excited States of Polyatomic Molecules Volume II*, (Academic Press, New York and London, 1974)
30. W.-C. Tam, C. E. Brion, J. Electron Spectrosc. Relat. Phenom. **3**, 263 (1974)

31. J. Doucet, P. Sauvegeau, C. Sandorfy, Chem. Phys. Lett., **19**, 316 (1973)
32. L. J. Bremner, M. G. Curtis, I. C. Walker, J. Chem. Soc. Faraday Trans. **87**, 1049 (1991)
33. A. Giuliani, J. Delwiche, S. V. Hoffmann, P. Limão-Vieira, N. J. Mason, M.-J. Hubin-Franskin, J. Chem. Phys. **119**, 3670 (2003)
34. J. Delwiche, P. Natalis, J. Momigny, J. E. Collin, J. Electron Spec. Relat. Phenom. **1**, 219 (1972)
35. D. R. Lide (Editor), in *Handbook of Chemistry and Physics* (CRC Press, New York,1992)
36. J. H. D. Eland, in *Photoelectron spectroscopy* (Butterworth & Co Ltd., London, 1984)
37. A. R. Milosavljević, S. Madžunkov, D. Šević, I. Čadež, B. P. Marinković, J. Phys. B: At. Mol. Opt. Phys. **39**, 609 (2006)
38. C. Hampel, K. Peterson, H.-J. Werner, Chem. Phys. Lett. **190**, 1 (1992).
39. MOLPRO, a package of ab initio programmes designed by H.-J. Werner and P. J. Knowles, version 2006.1, R. D. Amos, A. Bernhardsson, A. Berning, P. Celani, D. L. Cooper, M. J. O. Deegan, A. J. Dobbyn, F. Eckert, C. Hampel, G. Hetzer, P. J. Knowles, T. Korona, R. Lindh, A. W. Lloyd, S. J. McNicholas, F. R. Manby, W. Meyer, M. E. Mura, A. Nicklass, P. Palmieri, R. Pitzer, G. Rauhut, M. Schütz, U. Schumann, H. Stoll, A. J. Stone, R. Tarroni, T. Thorsteinsson, H.-J. Werner.
40. K. Kaufmann, W. Baumeister, M. Jungen, *J. Phys. B* **22**, 2223 (1989)
41. J. V. Ortiz, V. G. Zakrzewski, O. Dolgounircheva, in *Conceptual Perspectives in Quantum Chemistry*, Edited by J.-L. Calais and E. Kryachko (Kluwer Academic, 1997)
42. J. V. Ortiz, J. Chem. Phys. **89**, 6348 **(**1988)
43. M. J. Frisch, G. W. Trucks, H. B. Schlegel, G. E. Scuseria, M. A. Robb, J. R. Cheeseman, J. A. Montgomery Jr, T. Vreven, K. N. Kudin, J. C. Burant, J. M. Millam, S. S. Iyengar, J. Tomasi, V. Barone, B. Mennucci, M. Cossi, G. Scalmani, N. Rega, G. A. Petersson, H. Nakatsuji, M. Hada, M. Ehara, K. Toyota, R. Fukuda, J. Hasegawa, M. Ishida, T. Nakajima, Y. Honda, O. Kitao, H. Nakai, M. Klene, X. Li, J. E. Knox, H. P. Hratchian, J. B. Cross, V. Bakken, C. Adamo, J. Jaramillo, R. Gomperts, R. E. Stratmann, O. Yazyev, A. J. Austin, R. Cammi, C. Pomelli, J. W. Ochterski, P. Y. Ayala, K. Morokuma, G. A. Voth, P. Salvador, J. J. Dannenberg, V. G. Zakrzewski, S. Dapprich, A. D. Daniels, M. C. Strain, O. Farkas, K. D. Malick, A. D. Rabuck, K. Raghavachari, J. B. Foresman, J. V Ortiz, Q. Cui, A. G. Baboul, S. Clifford, J. Cioslowski, B. B. Stefanov, G. Liu, A. Liashenko, P. Piskorz, I. Komaromi, R. L. Martin, D. J. Fox, T. Keith, M. A. Al-Laham, C. Y. Peng, A. Nanayakkara, M. Challacombe, P. M. W. Gill, B. Johnson, W. Chen, M. W. Wong, C. Gonzalez, J. A. Pople, Gaussian 03, Revision D.01. Gaussian, Inc., Wallingford CT, (2004)
44. P. Luger, J. Buschmann, Angew. Chem. **95**, 423 (1983)
45. W. I. F. David, R. M. Ibberson, Acta Crystallogr., Sect. C **48**, 301 (1992)
46. E. Gallinella, B. Cadioli, J.-P. Flament, G. Berthier, J. Mol. Struct. (THEOCHEM) **315**, 137 (1994)
47. Y. Morino, K. Kuchistu, J. Chem. Phys. **20**,1809 (1952)
48. K. Kimura, S. Katsuwata, Y. Achiba, T. Yamazaki, S. Iwata, in *Handbook of HeI Photoelectron Spectra of fundamental Organic Molecules* (Halsted Press, New York, 1981)
49. M. Yamauchi, H. Yamakado, K. Ohno, J. Phys. Chem. A **101**, 6184 (1997)
50. X. G. Ren, C. G. Ning, J. K. Deng, S. F. Zhang, G. L. Su, F. Huang, G. Q. Li, Rev.

Sci. Instrum. **76**, 063103 (2005)

7. Figure Captions

Figure 1. (a) Structure of THF with atom numbering. (b) Pseudorotation of THF. Half of the cycle of the pseudorotation angle (ϕ = 0 to 180°) is shown. Picture adapted from references 17 and 25.

Figure 2. High-resolution photoabsorption spectrum (a) and electron energy loss spectrum (b) of THF recorded at 100 eV and 10° scattering angle.

Figure 3. High-resolution photoabsorption spectrum of THF (full lines) and theoretical calculations (vertical lines). The circles refer to the C_2 geometry and the triangles to the C_s one. (a). Detail of the 3s transition region and the associated vibrational progressions. (b) Detail of the 3p and 3d transitions and associated vibrational progressions. The trace of the first band of the photoelectron spectrum is shown in dots.

Figure 4. High-resolution photoabsorption spectrum of THF in the 8.2-10.6 eV showing Rydberg states and vibrational progressions.

Figure 5. He(I) photoelectron spectrum of THF (a) in the 8-16 eV energy region, (b) detail of the first band in the 9.1-10.6 eV energy region.

8. Table Captions

Table 1. Pseudorotation angle (in degree), symmetry and description of the potential energy surface minima for THF as determined from experiments and theoretical calculations.

Table 2. Experimental vertical excitation energies (eV) compared to theoretical transition energies (eV) and oscillator strength calculated for the C_2 and C_s conformers of THF.

Table 3. Comparison of the vibrational progressions found for THF for the neutral electronic ground states, the neutral electronic excited states and the ionic electronic ground state. Wavenumber are those of table 2 (in cm^{-1}).

Table 4. Rydberg series analysis. Energies in eV. Quantum defects are calculated according to the Rydberg formula, see text.

Table 5. Experimental ionisation energies and band assignments for THF.

Table 1. Pseudorotation angle (in degree), symmetry and description of the potential energy surface minima for THF as determined from experiments and theoretical calculations.

	Global minimum			Local minimum		
Experiments	ϕ	Conform.	Symmetry	ϕ	Conform.	Symmetry
MW [a]						
Engerholm *et al.* [18]	56	$\sim {}_5E$	C_1			
Meyer *et al.* [19]	52.5	$\sim {}_5E$	C_1			
Mamleev *et al.* [20]	90	$\breve{}_4I$	C_2	0, 180	${}_1E$, ${}^1E$	C_s
Melnik *et al.* [21]	90	$\breve{}_4I$	C_2	0, 180	${}_1E$, ${}^1E$	C_s
EMS [b]						
Yang *et al.* [25]		${}_1E$	C_s			
Theory						
This Work	90	$\breve{}_4I$	C_2	0, 180	${}_1E$, ${}^1E$	C_s
Cadioli *et al.* [22]	90	$\breve{}_4I$	C_2	0, 180	${}_1E$, ${}^1E$	C_s
Han and Kang [23]	90	$\breve{}_4I$	C_2	0,180	${}_1E$, ${}^1E$	C_s
Wu and Cremer [16]	90	$\breve{}_4I$	C_2			
Rayón and Sordo [24]	0	${}_1E$	C_s	90	$\breve{}_4I$	C_2

[a] Microwave spectroscopy. [b] Electron momentum spectroscopy.

Table 2. Experimental vertical excitation energies (eV) compared to theoretical transition energies (eV) and oscillator strength calculated for the C_2 and C_s conformers of THF.

E	Conformation	Symmetry	f ($x10^{-2}$)	$<r^2>$	HOMO [c]	SHOMO [d]	HOMO-2 [e]	Exp.
6.357	C_2	B	0.6	111	3s			6.221 [a]
6.608	C_s	A′	1.3	108	3s			6.353 [a]
6.889	C_2	A	0.04	126	3p			—
7.025	C_2	A	0.02	140	3p			—
7.103	C_2	B	0.2	138	3p			6.898 [a]
7.154	C_s	A′	4.7	127	3p			7.142 [a]
7.296	C_s	A″	0.3	140	3p			7.300 [a]
7.381	C_s	A′	0.7	144	3p			7.350 [v]
7.474	C_2	B	0.9	143	3d			7.483 [v]
7.713	C_2	A	0.002	170	3d			—
7.715	C_2	B	1.67	184	3d			7.730 [a]
7.724	C_s	A′	0.37	143	3d			7.749 [a]
7.754	C_2	B	2.07	179	3d			7.813 [a]
7.859	C_2	A	0.06	198	3d			—
7.978	C_s	A″	0.28	169	3d			—
7.985	C_s	A′	1.5	183	3d			7.867 [a]
7.988	C_2	B	0.05	293	4s			—
8.017	C_s	A″	0.72	180	3d			—
8.103	C_s	A′	0.02	196	3d			—
8.144	C_2	A	0.02	372	4p			—
8.188	C_2	B	0.01	369	4p			—
8.194	C_2	A	0.00003	405	4s			
8.249	C_s	A′	0.18	285	4s			
8.288	C_2	A	1.12	120		3s		8.3 [v]
8.335	C_2	B	0.17	454	4d			8.515 [v]
8.405	C_s	A′	0.97	369	4p			8.37 [v]
8.422	C_2	B	0.23	558	4d			8.533 [v]
8.439	C_2	A	0.002	530	4d			
8.451	C_s	A″	0.095	393	4p			
8.457	C_2	B	1.13	558	4d			8.557 [v]
8.460	C_s	A′	0.61	345	4p			8.4 [v]
8.494	C_s	A′	0.16	170			3s	
8.496	C_2	A	0.003	598	4d			
8.545	C_2	B	0.038	770	5s			
8.584	C_s		0.007	443	4d			
8.615	C_2	A	0.0008	975	5p			
8.623	C_2	B	0.0033	907	5p			
8.635	C_2	A	0.0003	1019	5p			

8.684	C_s	A″	0.0012	140		3s		
8.693	C_s	A′	0.40	550	4d			8.652 [v]
8.700	C_s	A″	0.12	527	4d			8.695 [v]
8.715	C_2	B	0.03	1030	5d			
8.720	C_s	A″	0.19	555	4d			8.719 [v]
8.751	C_s	A′	0.005	591	4d			
8.760	C_2	B	0.055	1244	5d			
8.792	C_2	B	0.6	180		3p		8.793 [v]
8.800	C_2	A	0.006	839	5d			
8.808	C_s	A′	0.063	752	5s			
8.824	C_2	B	1.11	887	5d			8.875 [v]
8.842	C_2	B	0.0265	1546	6s			
8.850	C_2	A	0.0092	835	5d			
8.857	C_2	A	0.00015	1713	6p			
8.861	C_2	A	0.0017	1560	6p			
8.872	C_s	A′	0.322	937	5p			8.888 [v]
8.881	C_2	B	0.239	1210	6p			
8.889	C_2	B	0.477	607		3p		8.844 [v]
8.899	C_s	A′	0.206	985	5p			8.939 [v]
8.901	C_s	A″	0.040	1013	5p			
8.928	C_2	A	0.028	281	σ*			
8.934	C_2	A	0.004	377		3p		
8.965	C_s	A′	0.003	1032	5d			
8.966	C_2	A	0.308	198			3s	8.965 [v]
9.014	C_s	A′	0.738	519	5d			9.024 [v]
9.039	C_s	A″	2.43	172			3p	9.137 [v]
9.040	C_s	A′	0.103	775	5d			
9.064	C_s	A″	0.020	877	5d			
9.081	C_s	A″	0.474	820	5d			8.991 [v]

[a] stands for adiabatic and [v] stands for vertical.
[c] HOMO: 9b for C_2 and 12a' for C_s. [d] SHOMO: 11a for C_2 and 8a" for C_s. [e] HOMO-2: 10a for C_2 and 11a' for C_s.

Table 3. Comparison of the experimental vibrational progressions found for THF for the neutral electronic ground states, the neutral electronic excited states with both present theoretical (MP2/aug-cc-pVDZ) and experimental vibrational progressions found for the ionic electronic ground state. Wavenumber are those of supplementary information table 2 (in cm^{-1}).

	Neutral									Ionic	
Mode	Ground A´ / A	3s(C_2) B	3s(C_s) A'	3p(C_2) B	3p(C_s) A´	3p(C_s) A˝	3p(C_s) A´	3d(C_2) B	3d(C_2) B	Theory Ground A/B	Exp. Ground A / B
ν_{33}	39.5 [a]	62.9	171	183.9	79.8	136.3	185.5				
ν_{17}	286		237								
ν_{26}	1244							1268.7	1296.9	1243.3	1234.0
ν_{32}	591								542.0 [b]	570.6	596.8 [b]
ν_{11}	1142								1135.6	1042.1	1064.7 [b]

[a] Estimation from Ref. 22. [b] Deduced from combinations, see text.

Table 4. Rydberg series analysis. Energies in eV. Quantum defects are calculated according to the Rydberg formula, see text.

1^{st} ionic limit (EI = 9.433 eV)					
	C_2			C_s	
En		δ	En		δ
	ns			**ns**	
6.221	3	0.942	6.353	3	0.898
	np			**np**	
6.8976	3	0.683	7.142	3	0.563
			7.30	3	0.474
			7.350	3	0.444
			8.37	4	0.422
			8.4	4	0.371
			8.888	5	0.004
			8.939	5	-0.248
	nd			**nd**	
7.483	3	0.359	7.749	3	0.158
7.730	3	0.174	7.867	3	0.052
7.813	3	0.102			
8.515	4	0.149	8.652	4	-0.174
8.533	4	0.119	8.695	4	-0.292
8.557	4	0.060	8.719	4	-0.365
8.875	5	0.062	8.991	5	-0.548
			9.024	5	-0.765
9.037	6	0.141	9.130	6	-0.700
9.143	7	0.146	9.164	7	-0.108
9.211	8	0.166			
9.253	9	0.315			

2^{nd} ionic limit (EI = 11.512 eV)		
	C_2	
En		δ
	ns	
8.30	3	0.942
	np	
8.793	3	0.763
8.844	3	0.742
	nd	
9.96	3	0.039

3^{rd} ionic limit (EI = 11.964 eV)					
	C_2			C_s	
En		δ	En		δ
	ns				
8.965	3	0.870			
				np	
			9.037	3	0.655

Table 5. Calculated and experimental ionisation energies and band assignments for THF.

Theory						Experiment			
This work				Yang *et al.* [25]		This work	Yang *et al.* [25]	Kimura *et al.* [48]	Yamauchi *et al.* [49]
OVGF/aug-cc-pVDZ		OVGF 6-31G*		SAOP ET-PVQZ		PES [a]	EMS [b]	PES [b]	PIS [c]
C_2	C_s	C_2	C_s	C_2	C_s				
9.94 (9b)	9.91 (12a')	9.38	9.63	10.01 (9b)	10.32 (12a')	9.718	9.7	9.74	9.67
11.65 (11a)	11.89 (8a")	11.11	11.36	11.67 (11a)	11.93 (11a')	11.515	11.9	11.52	11.41
12.20 (10a)	11.65 (11a')	11.85	11.65	12.11 (10a)	11.97 (8a")	11.964			11.99
12.43 (8b)	12.26 (7a")	12.08	11.86	12.51 (8b)	12.40 (7a")	12.466			12.48
12.62 (9a)	12.30 (10a')	12.30	12.11	12.75 (9a)	12.72 (6a")	12.868		12.52	12.90
14.21 (7b)	13.74 (6a")	14.06	13.69	13.98 (7b)	13.84 (9a')	14.040	14.1	14.1	14.00
14.82 (6b)	14.49 (9a')	14.72	14.28	14.48 (8a)	14.23 (5a")	14.430		14.5	14.45
14.95 (8a)	15.29 (5a")	14.72	15.13	14.76 (6b)	15.12 (8a')	15.271		15.4	15.29
16.57 (7a)	16.29 (8a')	16.54	16.15	16.22 (7a)	15.99 (7a')	16.246	16.3	16.8	16.70
16.93 (5b)	16.83 (7a')	16.91	16.66	16.51 (5b)	16.31 (4a")				16.70
				18.64 (6a)	18.67 (6a')		19.3	19.5	19.42

[a] He(I) Photoelectron spectroscopy, [b] Electron Momentum Spectroscopy, [c] Penning Ionisation Spectroscopy.

Figure 1. (a) Structure of THF with atom numbering. (b) Pseudorotation of THF. Half of the cycle of the pseudorotation angle (ϕ = 0 to 180°) is shown. Picture adapted from references 17 and 25.

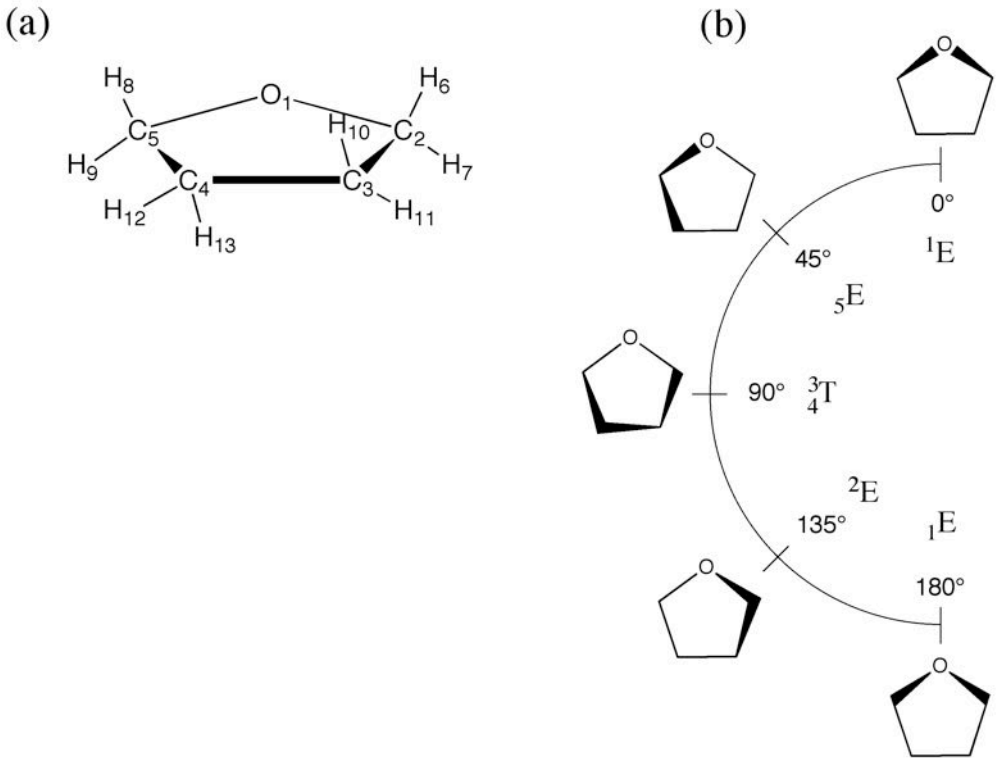

Figure 2. High-resolution photoabsorption spectrum (a) and electron energy loss spectrum (b) of THF recorded at 100 eV and 10° scattering angle.

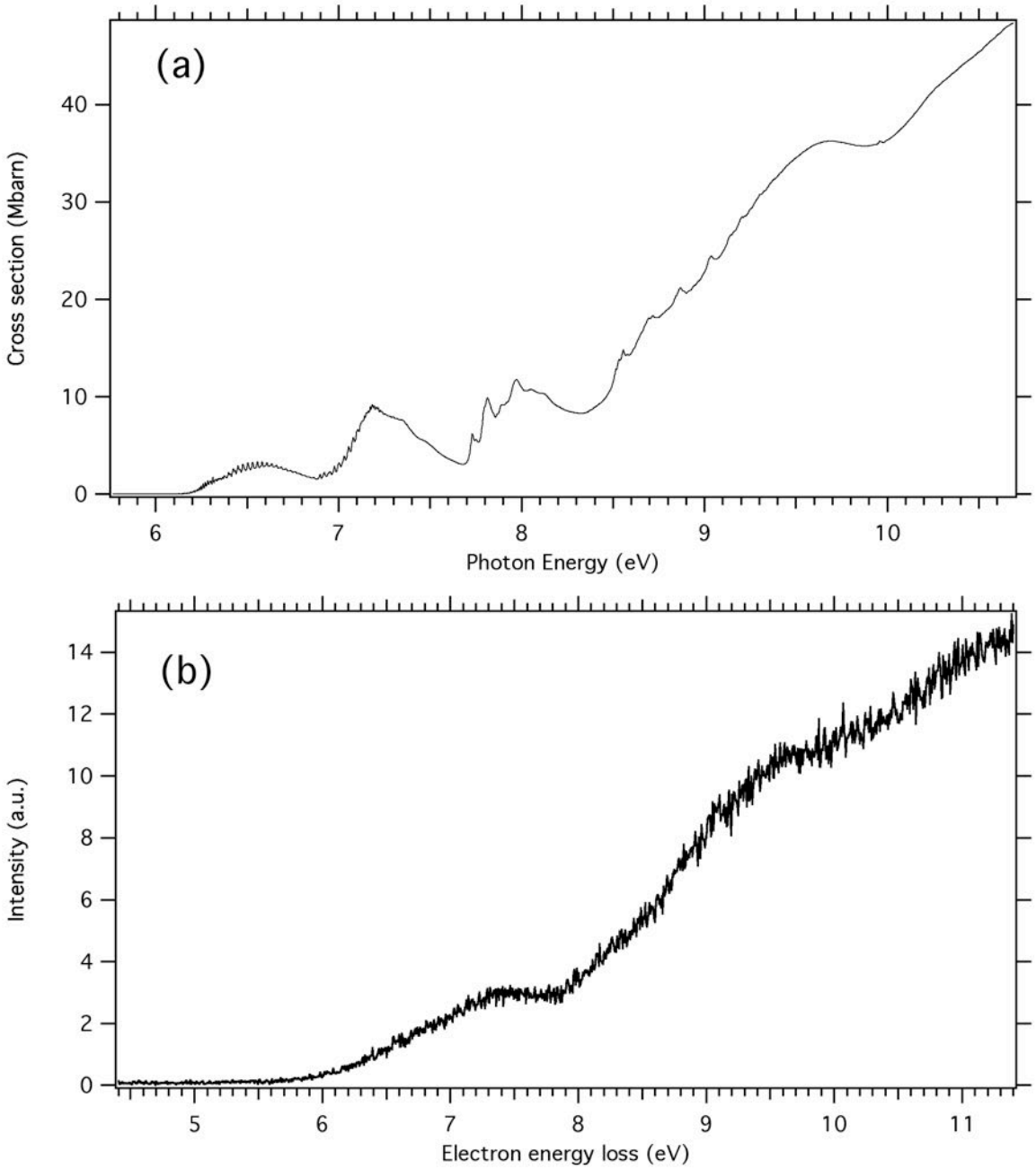

Figure 3. High-resolution photoabsorption spectrum of THF (full lines) and theoretical calculations (vertical lines). The circles refer to the C_2 geometry and the triangles to the C_s one. (a). Detail of the 3s transition region and the associated vibrational progressions. (b) Detail of the 3p and 3d transitions and associated vibrational progressions. The trace of the first band of the photoelectron spectrum is shown in dots.

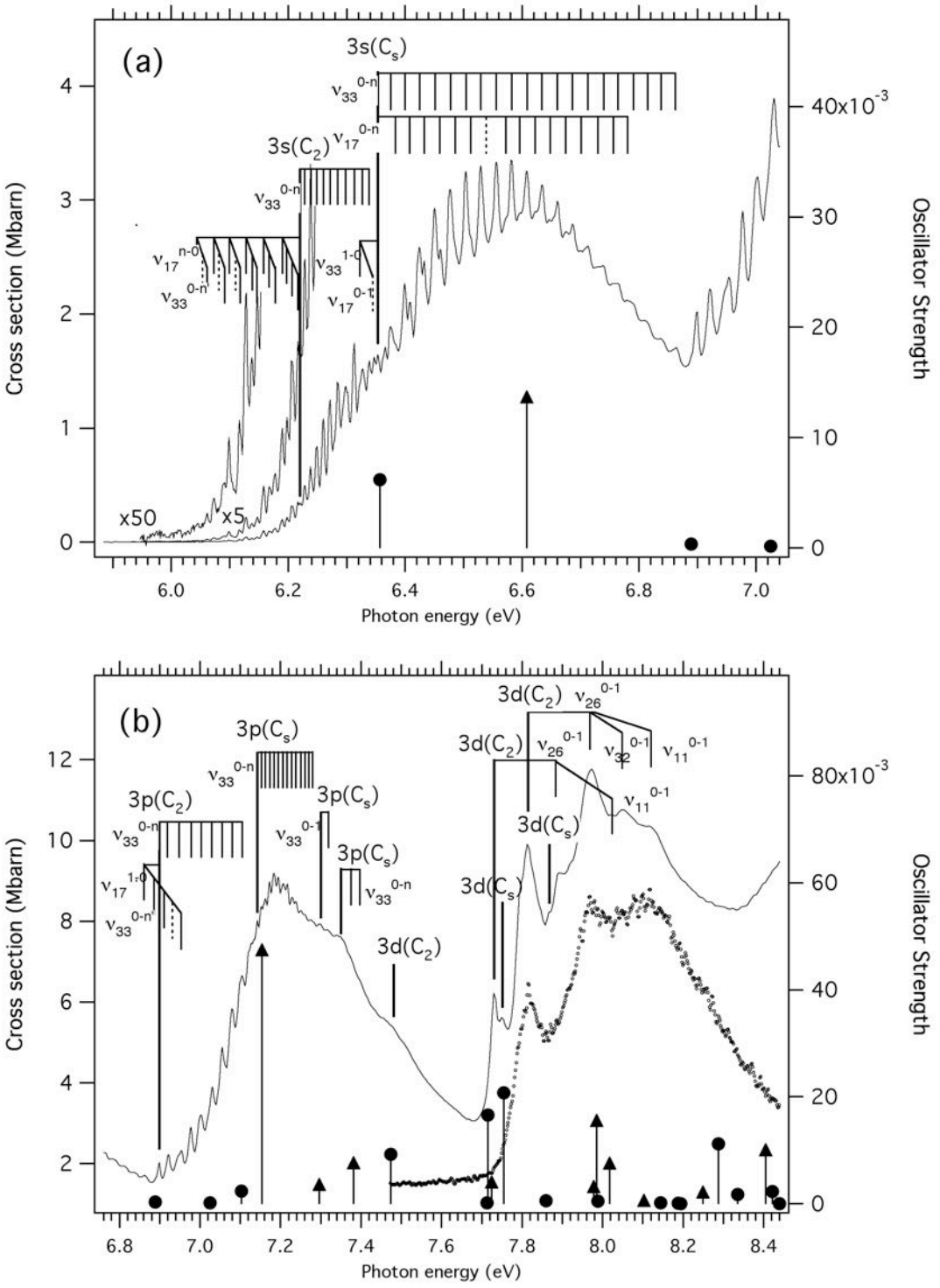

Figure 4. High-resolution photoabsorption spectrum of THF in the 8.2-10.6 eV showing Rydberg states and vibrational progressions.

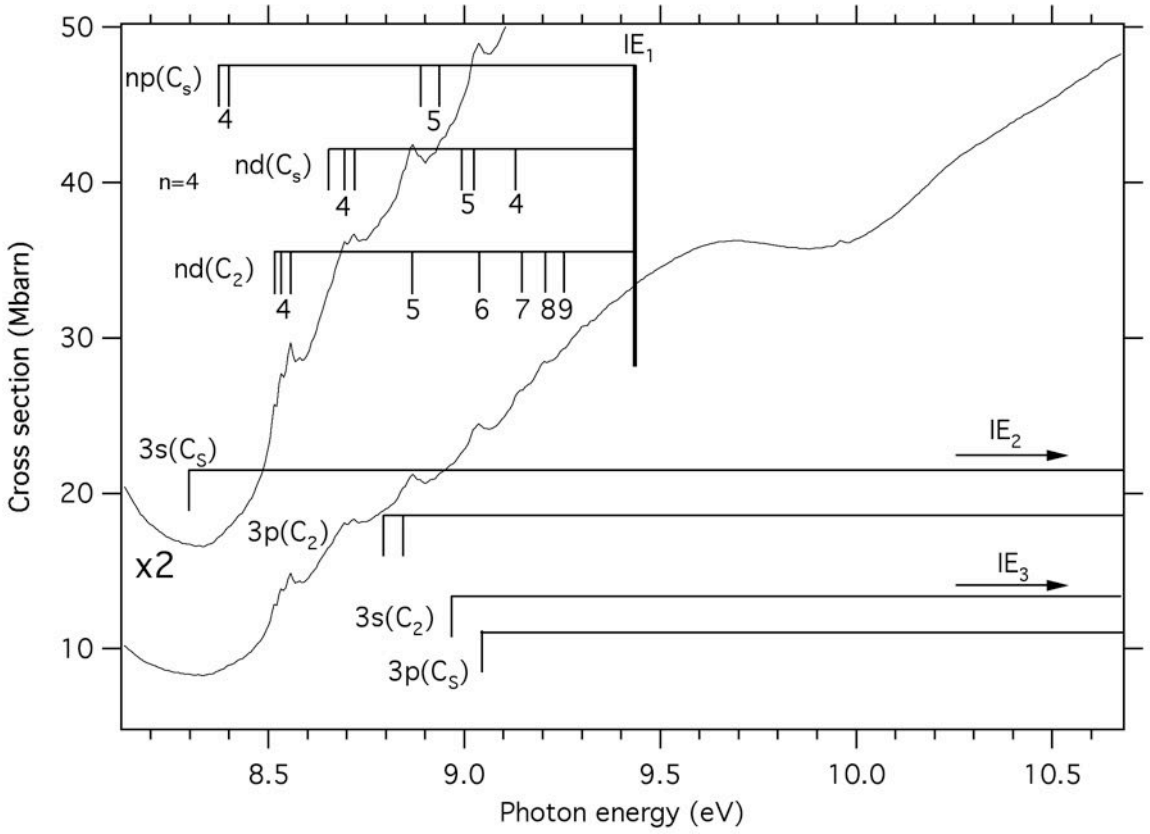

Figure 5. He(I) photoelectron spectrum of THF (a) in the 8-16 eV energy region, (b) detail of the first band in the 9.1-10.6 eV energy region.

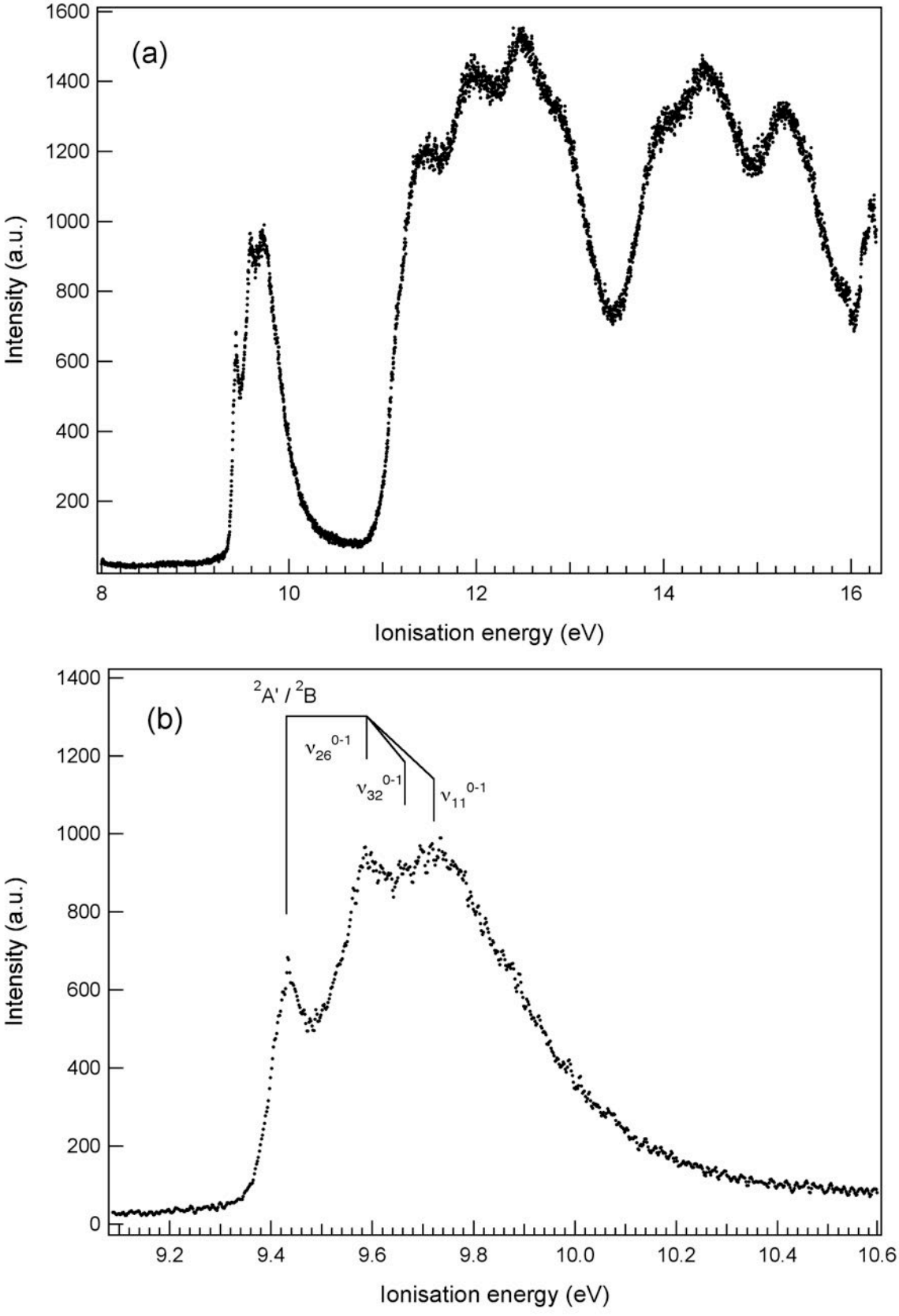

9. Supplementary Information

Table captions

Supplementary information table 1. Theoretical and experimental structural parameters for neutral and ionised tetrahydrofuran . Bond lengths and angles are in Å and degree, respectively.

Supplementary information table 2. Fundamental vibrational frequencies for C_2 tetrahydrofuran.

Supplementary information table 3. Vibrational structure in the 3s band system (6 - 6.8 eV).

Supplementary information table 4. Vibrational structure in the 3p band system (6.8 – 7.4 eV).

Supplementary information table 5. Vibrational structure in the 3d band system (7.4 – 8.2 eV).

Supplementary information table 6. MP2/aug-cc-pVDZ harmonic vibrational frequencies for the ground ionic state of C_2 and C_{2v} conformers of tetrahydrofuran .

Supplementary information table 7. Vibrational structure for the ionic ground state.

Supplementary information table 1. Theoretical and experimental structural parameters for neutral and ionised tetrahydrofuran . Bond lengths and angles are in Å and degree, respectively.

Parameter	Positive ion				Neutral molecule								
	UMP2		MP2		MP2		B3LYP		MP2		MW [a]	X-ray [b]	ND [c]
	aug-cc-pVDZ		aug-cc-pVDZ		6-31G*		6-31G**		aug-cc-pVTZ				
	This work		This work		Ref. 22		Ref. 16		Ref. 24		Ref. 19	Ref. 44	Ref. 45
	C_s	C_{2v}	C_2	C_s	C_2	C_s	C_2	C_s	C_2	C_s	C_1	C_2	C_2
O_1-C_2	1.433	1.443	1.448	1.437	1.4353	1.4253	1.432	1.423	1.434	1.424	1.427	1.435(5)	1.438(3)
C_2-C_3	1.529	1.525	1.532	1.543	1.5258	1.5367	1.534	1.545	1.523	1.533	1.5519(27)	1.531(10)	1.516(3)
C_4-C_5	1.529	1.525	1.532	1.543					1.523	1.533	1.5239(26)		
C_3-C_4	1.561	1.543	1.538	1.543	1.5280	1.5468	1.536	1.554	1.527	1.546	1.53324(69)	1.531(10)	1.516(3)
C_5-H_8	1.110	1.116	1.101	1.098	1.0996	1.0928	1.096	1.093	1.094	1.097	1.09626(60)	1.09(5)	1.101(4) [d]
C_5-H_9	1.110	1.101	1.105	1.108	1.0952	1.1021	1.093	1.103	1.089	1.087	1.09372(60)	1.09(5)	1.094(4) [d]
C_4-H_{12}	1.097	1.098	1.102	1.099	1.0942	1.0933	1.095	1.093	1.088	1.088	1.095	1.09(5)	1.094(4) [d]
C_4-H_{13}	1.097	1.100	1.100	1.100	1.0957	1.0941	1.101	1.094	1.088	1.088	1.095	1.09(5)	1.096(4) [d]
$C_2O_1C_5$	112.02	109.93	109.17	103.98	109.30	104.10	109.9	105.5	109.33	104.07		109.8(3)	109.9(3)
$O_1C_2C_3$	108.52	106.25	106.10	105.34	106.17	105.34	106.5	105.7	106.09	105.37		106.7(4)	106.4(2)
$C_2C_3C_4$	105.47	101.87	101.17	103.25	101.12	103.19	101.5	103.3	101.09	103.17		101.9(3)	102.6(2)
$O_1C_2H_8$	103.09	101.03	108.94	107.58	109.32	109.98							108.1(2)
$O_1C_2H_9$	103.09	105.94	108.08	109.44	108.38	107.68							108.4(3)
$C_2O_1C_5C_4$	-12.01	0.00	-12.95	42.55	-12.88	42.58	-12.0	40.2	-12.96	42.60		-11.7(3)	-11.3(2)
$O_1C_2C_3C_4$	30.47	0.00	33.07	-25.33	32.94	-25.30	30.8	23.7	33.08	-25.32		29.6(3)	28.8(2)
$C_2C_3C_4C_5$	-36.45	0.00	-39.35	0.00	-39.07	0.00	-36.5	0.0	-39.31	0.00		-35.2(4)	-34.5(2)

[a] Microwave spectroscopy. [b] X-Ray diffraction data at 148 K. [c] High resolution neutron diffraction at 5K. [d] Bond length for CD, average geometrical parameters.

Supplementary information table 2. Fundamental vibrational frequencies for C_2 tetrahydrofuran.

A symmetry	Description	Wavenumber (cm^{-1})	Energy (meV)
ν_1	β-CH_2 symmetric stretch	2962	367.2
ν_2	α-CH_2 asymmetric stretch	2941	364.6
ν_3	β-CH_2 symmetric stretch	2913	361.2
ν_4	α-CH_2 symmetric stretch	2875	356.5
ν_5	α- and β-CH_2 bend	1488	184.5
ν_6	β-CH_2 bend	1462	181.3
ν_7	α-CH_2 wag	1364	169.1
ν_8	β-CH_2 wag + β-CH_2 twist	1308	162.2
ν_9	α- and β-CH_2 twist	1227	152.1
ν_{10}	β-CH_2 twist + β-CH_2 wag + ...	1178	146.1
ν_{11}	α-CH_2 rock + β-CH_2 rock	1142	141.6
ν_{12}	$C_\alpha C_\beta$ symmetric stretch + β-CH_2 wag	1029	127.6
ν_{13}	$C_\beta C_\beta$ stretch + $C_\alpha C_\beta$ symmetric stretch	919	113.9
ν_{14}	COC symmetric stretch	895	111.0
ν_{15}	β- and α-CH_2 rock	840	104.1
ν_{16}	Ring bend	657	81.5
ν_{17}	Ring pucker	286	35.5
B symmetry			
ν_{18}	β-CH_2 asymmetric stretch	2972	368.5
ν_{19}	α-CH_2 asymmetric stretch	2934	363.8
ν_{20}	β-CH_2 symmetric stretch	2912	361.0
ν_{21}	α-CH_2 symmetric stretch	2858	354.3
ν_{22}	α-CH_2 bend	1477	183.1
ν_{23}	β-CH_2 bend	1449	179.7
ν_{24}	α- and β-CH_2 wag	1334	165.4
ν_{25}	β- and α-CH_2 wag	1292	160.2
ν_{26}	β- and α-CH_2 twist	1244	154.2
ν_{27}	α-CH_2 twist + α-CH_2 rock	1162	144.1
ν_{28}	COC asymmetric stretch	1070	132.7
ν_{29}	β-CH_2 rock + $C_\alpha C_\beta$ asymmetric stretch	955	118.4
ν_{30}	$C_\alpha C_\beta$ asymmetric stretch + β-CH_2 twist	910	112.8
ν_{31}	β-CH_2 rock + ring bend	865	107.2
ν_{32}	Ring bend + β-CH_2 rock	591	73.3
ν_{33}	Ring pucker & β-CH_2 twist. Pseudo rotation.	(39.5) [a]	(5)

Assignments from Lepage *et al.* Ref. [4]
All frequencies taken from Ref. 22.
[a] Estimation of the pseudo rotational mode ν_{33} see Ref. 22

Supplementary information table 3. Vibrational structure in the 3s band system (6 - 6.8 eV).

Energy	Energy difference [a]	Vibrational Spacing [b]		Energy Previous work Ref. 28	Assignations Previous work Ref. 28	Assignation This work.
eV	meV	meV	cm^{-1}	eV		
6.043	-177.4	-29.6	-238.7	6.047	ν_6^0	ν_{17}^{6-0}
6.061	-159.7	15	121.0	6.061	—	$\nu_{17}^{6-0} + \nu_{33}^{0-2}$
6.073	-147.8	-25.4	-204.7	6.071	ν_5^0	ν_{17}^{5-0}
6.091	-129.9	17.9	144.4	6.090	—	$\nu_{17}^{5-0} + \nu_{33}^{0-2}$
6.099	-122.4	-28.6	-230.7	6.100	ν_4^0	ν_{17}^{4-0}
6.117	-104.4	18.0	145.2	6.117	—	$\nu_{17}^{4-0} + \nu_{33}^{0-2}$
6.127	-93.8	30.5	-246.0	6.129	ν_3^0	ν_{17}^{3-0}
6.138	-83.2	10.6	85.49	6.136	ν_3^1	$\nu_{17}^{3-0} + \nu_{33}^{0-1}$
6.147	-74.0	9.2	74.20	6.146	ν_3^2	$\nu_{17}^{3-0} + \nu_{33}^{0-2}$
6.158	-63.3	-32.2	-259.7	6.159	ν_2^0	ν_{17}^{2-0}
6.169	-54.2	9.1	73.40	6.167	ν_2^1	$\nu_{17}^{2-0} + \nu_{33}^{0-1}$
6.178	-43.4	10.8	87.11	6.175	ν_2^2	$\nu_{17}^{2-0} + \nu_{33}^{0-2}$
6.190	-31.1	-31.1	-250.8	6.190	ν_1^0	ν_{17}^{1-0}
6.198	-23.3	7.8	62.91	6.198	ν_1^1	$\nu_{17}^{1-0} + \nu_{33}^{0-1}$
6.207	-14.0	9.3	75.01	6.207	ν_1^2	$\nu_{17}^{1-0} + \nu_{33}^{0-2}$
6.216	-4.7	9.3	75.01	6.217	ν_1^3	$\nu_{17}^{1-0} + \nu_{33}^{0-3}$
6.221	0	0	0	6.222	0_0^0	$3s(C_2)$
				6.228	ν_1^4	
6.229	7.8	7.8	62.91	6.230	ν_0^1	ν_{33}^{0-1}
6.238	17.2	9.4	75.82	6.239	ν_0^2	ν_{33}^{0-2}
6.249	28.2	11	88.72	6.249	ν_0^3	ν_{33}^{0-3}
6.260	39.3	11.1	89.53	6.260	ν_0^4	ν_{33}^{0-4}
6.271	42.5	11	88.72	6.272	ν_0^5	ν_{33}^{0-5}
6.284	63	12.7	102.4	6.285	ν_0^6	ν_{33}^{0-6}
6.298	77.4	14.4	116.1	6.297	ν_0^7	ν_{33}^{0-7}
6.313	84	14.4	116.1	6.313	ν_0^8	ν_{33}^{0-8}
6.323	-30.8	-30.8	-248.4			ν_{17}^{1-0}
6.327	98.5	14.5	116.9	6.328	ν_0^9	ν_{33}^{0-9}
6.339	117.7	11.4	91.95	6.343	ν_0^{10}	ν_{33}^{0-10}
6.353	0	0	0			$3s(C_s)$
6.375	21.2	21.2	171.0			ν_{33}^{0-1}
6.383	29.4	29.4	237.1			ν_{17}^{0-1}
6.399	45.9	24.7	199.2			ν_{33}^{0-2}
6.409	55.8	26.4	212.9			ν_{17}^{0-2}
6.424	70.8	24.9	200.8			ν_{33}^{0-3}
6.432	79.1	23.3	187.9			ν_{17}^{0-3}
6.451	97.5	26.7	215.3			ν_{33}^{0-4}
6.461	107.6	28.5	229.8			ν_{17}^{0-4}
6.476	122.8	25.3	204.1			ν_{33}^{0-5}

6.486	132.9	25.3	204.1	$\nu_{17}^{0\text{-}5}$
6.503	149.9	27.1	218.6	$\nu_{33}^{0\text{-}6}$
6.512	158.5	25.6	206.5	$\nu_{17}^{0\text{-}6}$
6.529	175.6	25.7	207.3	$\nu_{33}^{0\text{-}7}$
6.546	194.6	36.1	291.2	$\nu_{17}^{0\text{-}7}$
6.557	203.2	27.6	222.6	$\nu_{33}^{0\text{-}8}$
6.570	217.1	22.5	181.5	$\nu_{17}^{0\text{-}8}$
6.581	227.6	24.4	196.8	$\nu_{33}^{0\text{-}9}$
6.597	243.4	26.3	212.1	$\nu_{17}^{0\text{-}9}$
6.607	253.9	26.3	212.1	$\nu_{33}^{0\text{-}10}$
6.623	269.8	26.4	212.9	$\nu_{17}^{0\text{-}10}$
6.634	280.4	26.5	213.7	$\nu_{33}^{0\text{-}11}$
6.646	292.9	23.1	186.34	$\nu_{17}^{0\text{-}11}$
6.661	307.2	26.8	216.2	$\nu_{33}^{0\text{-}12}$
6.675	321.5	28.6	230.7	$\nu_{17}^{0\text{-}12}$
6.687	334.1	26.9	217.0	$\nu_{33}^{0\text{-}13}$
6.700	346.8	25.3	204.1	$\nu_{17}^{0\text{-}13}$
6.713	359.4	25.3	204.1	$\nu_{33}^{0\text{-}14}$
6.727	374	27.2	219.4	$\nu_{17}^{0\text{-}14}$
6.740	386.8	27.4	221.0	$\nu_{33}^{0\text{-}15}$
6.755	401.5	27.5	221.8	$\nu_{17}^{0\text{-}15}$
6.766	412.5	25.7	207.3	$\nu_{33}^{0\text{-}16}$
6.779	425.5	24	193.6	$\nu_{17}^{0\text{-}16}$
6.790	436.6	24.1	194.4	$\nu_{33}^{0\text{-}17}$
6.816	462.8	26.2	211.3	$\nu_{33}^{0\text{-}18}$
6.837	483.4	20.6	166.2	$\nu_{33}^{0\text{-}19}$
6.861	508	24.6	198.4	$\nu_{33}^{0\text{-}20}$

[a] The energy difference is calculated with respect to the electronic origin. Negative value indicates a hot band. [b] The vibrational spacing are the energy difference between two adjacent vibrational levels. Features from Ref. 28 labelled by — were reported in that work but not assigned.

Supplementary information table 4. Vibrational structure in the 3p band system (6.8 – 7.4 eV).

Energy	Energy difference [a]	Vibrational Spacing [b]		Assignation
eV	meV	meV	cm^{-1}	
6.863	-34.4	-34.4	-277.5	ν_{17}^{1-0}
6.890	-7.7	26.7	215.3	$\nu_{17}^{1-0}+\nu_{33}^{0-1}$
6.898	0	0	0	$3p(C_2)$
6.913	15.4	49.8	401.7	$\nu_{17}^{1-0}+\nu_{33}^{0-2}$
6.920	22.8	22.8	183.9	ν_{33}^{0-1}
6.945	47.4	24.6	198.4	ν_{33}^{0-2}
6.953	55.6	40.2	324.2	$\nu_{17}^{1-0}+\nu_{33}^{0-4}$
6.973	75	27.6	222.6	ν_{33}^{0-3}
7.001	103.2	28.2	227.4	ν_{33}^{0-4}
7.030	132.7	29.5	237.9	ν_{33}^{0-5}
7.055	157.4	24.7	199.2	ν_{33}^{0-6}
7.080	182	24.6	198.4	ν_{33}^{0-7}
7.105	207.5	25.5	205.7	ν_{33}^{0-8}
7.142	0	0	0	$3p(C_s)$
7.152	9.9	9.9	79.8	ν_{33}^{0-1}
7.163	21.4	11.5	92.8	ν_{33}^{0-2}
7.173	31.2	9.8	79.0	ν_{33}^{0-3}
7.183	41.1	9.9	79.8	ν_{33}^{0-4}
7.194	52.5	11.4	91.9	ν_{33}^{0-5}
7.206	64	11.5	92.8	ν_{33}^{0-6}
7.216	73.9	9.9	79.8	ν_{33}^{0-7}
7.227	85.4	11.5	92.7	ν_{33}^{0-8}
7.237	95.2	9.8	79.0	ν_{33}^{0-9}
7.250	108.3	13.1	105.7	ν_{33}^{0-10}
7.259	117.1	8.8	71.0	ν_{33}^{0-11}
7.274	132	14.9	120.2	ν_{33}^{0-12}
7.283	140.6	8.6	69.3	ν_{33}^{0-13}
7.3	0	0	0	$3p(C_s)$
7.317	16.9	16.9	136.3	ν_{33}^{0-1}
7.350	0	0	0	$3p(C_s)$
7.373	23	23	185.5	ν_{33}^{0-1}
7.396	46	23	185.5	ν_{33}^{0-2}

[a] The energy difference is calculated with respect to the electronic origin. Negative value indicates a hot band. [b] The vibrational spacing are the energy difference between two adjacent vibrational levels.

Supplementary information table 5. Vibrational structure in the 3d band system (7.4 – 8.2 eV).

Energy	Energy difference [a]	Vibrational Spacing [b]		Assignation [a]
eV	meV	meV	cm^{-1}	
7.730	0	0	0	$3d(C_2)$
7.813	0	0	0	$3d(C_2)'$
7.887	157.3	157.3	1268.7	$3d(C_2) + \nu_{26}^{0-1}$
7.973	160.8	160.8	1296.9	$3d(C_2)' + \nu_{26}^{0-1}$
8.025	295.2	157.9	1273.5	$3d(C_2) + \nu_{26}^{0-1} + \nu_{11}^{0-1}$
8.042	228	67.2	542.0	$3d(C_2)' + \nu_{26}^{0-1} + \nu_{32}^{0-1}$
8.114	301.6	384.4	3100.4	$3d(C_2)' + \nu_{26}^{0-1} + \nu_{11}^{0-1}$

[a] The energy difference is calculated with respect to the electronic origin. Negative value indicates a hot band. [b] The vibrational spacing are the energy difference between two adjacent vibrational levels.

Supplementary information table 6. MP2/aug-cc-pVDZ harmonic vibrational frequencies for the ground ionic state of C_2 and C_{2v} conformers of tetrahydrofuran .

Species	C_2 Wavenumber (cm^{-1})	Energy (meV)	Species	C_{2v} Wavenumber (cm^{-1})	Energy (meV)
A			A_1		
ν_1	3190.4	395.6	ν_1	3138.6	389.1
ν_2	3141.5	389.5	ν_2	3013.5	373.6
ν_3	3113.6	386.0	ν_3	1516.5	188.0
ν_4	2955.7	366.5	ν_4	1333.2	165.3
ν_5	1495.1	185.4	ν_5	1280.9	158.8
ν_6	1390.3	172.4	ν_6	1396.5	173.1
ν_7	1350.3	167.4	ν_7	1091.9	135.4
ν_8	1333.2	165.3	ν_8	930.1	115.3
ν_9	1188	147.3	ν_9	764.2	94.7
ν_{10}	1174.9	145.7	ν_{10}	733	90.9
ν_{11}	1042.1	129.2	A_2		
ν_{12}	998.3	123.8	ν_{11}	3190.5	395.6
ν_{13}	942.6	116.9	ν_{12}	3050.7	378.2
ν_{14}	805.9	99.9	ν_{13}	1271.1	157.6
ν_{15}	752.3	93.3	ν_{14}	1139.9	141.3
ν_{16}	613.4	76.1	ν_{15}	1003.3	124.4
ν_{17}	238.6	29.6	ν_{16}	646.1	80.1
			ν_{17}	i188.9	i23.4
B			B_1		
ν_{18}	3197.9	396.5	ν_{18}	3207.4	397.7
ν_{19}	3143.5	389.7	ν_{19}	3057.1	379.0
ν_{20}	3117.7	386.5	ν_{20}	1240	153.7
ν_{21}	2949.3	365.72	ν_{21}	1198	148.5
ν_{22}	1479.9	183.5	ν_{22}	905.1	112.2
ν_{23}	1399.2	173.5	ν_{23}	734	91.0
ν_{24}	1322.1	163.9	ν_{24}	83.6	10.4
ν_{25}	1285.8	159.4			
ν_{26}	1243.3	154.1	B_2		
ν_{27}	1136.1	140.9	ν_{25}	3132.1	388.3
ν_{28}	967.8	120.0	ν_{26}	2999.2	371.9
ν_{29}	905.3	112.2	ν_{27}	1491.8	185.0
ν_{30}	887.3	110.0	ν_{28}	1391.9	172.6
ν_{31}	709.9	88.0	ν_{29}	1341.8	166.4
ν_{32}	570.6	70.7	ν_{30}	1275.4	158.1
ν_{33}	213.8	26.5	ν_{31}	1009.2	125.1
			ν_{32}	767	95.1
			ν_{33}	694	86.0

Supplementary information table 7. Vibrational structure for the ionic ground state.

Energy eV	Energy difference [a] meV	Vibrational Spacing meV	Vibrational Spacing cm^{-1}	Assignation
9.433	0	0	0	0-0
9.586	153	153	1234.0	ν_{26}^{0-1}
9.66	227	74	596.8	$\nu_{26}^{0-1} + \nu_{32}^{0-1}$
9.718	285	132	1064.7	$\nu_{26}^{0-1} + \nu_{11}^{0-1}$

[a] The energy difference is calculated with respect to the electronic origin.